The chemical compositions of accreted and *in situ* galactic globular clusters according to SDSS/APOGEE

Danny Horta [,1]* Ricardo P. Schiavon,[1] J. Ted Mackereth [,1,2] Timothy C. Beers,[3]
José G. Fernández-Trincado,[4] Peter M. Frinchaboy,[5] D. A. García-Hernández,[6,7]
Doug Geisler,[8,9] Sten Hasselquist,[10,11] Henrik Jönsson [,12,13] Richard R. Lane,[14,15]
Steven R. Majewski,[16] Szabolcs Mészáros,[17,18] Christian Moni Bidin,[19]
David M. Nataf,[20] Alexandre Roman-Lopes,[21] Christian Nitschelm,[22]
J. Vargas-González [23] and Gail Zasowski[11]

Affiliations are listed at the end of the paper

ABSTRACT

Studies of the kinematics and chemical compositions of Galactic globular clusters (GCs) enable the reconstruction of the history of star formation, chemical evolution, and mass assembly of the Galaxy. Using the latest data release (DR16) of the SDSS/APOGEE survey, we identify 3090 stars associated with 46 GCs. Using a previously defined kinematic association, we break the sample down into eight separate groups and examine how the kinematics-based classification maps into chemical composition space, considering only α (mostly Si and Mg) elements and Fe. Our results show that (i) the loci of both *in situ* and accreted subgroups in chemical space match those of their field counterparts; (ii) GCs from different individual accreted subgroups occupy the same locus in chemical space. This could either mean that they share a similar origin or that they are associated with distinct satellites which underwent similar chemical enrichment histories; (iii) the chemical compositions of the GCs associated with the low orbital energy subgroup defined by Massari and collaborators is broadly consistent with an *in situ* origin. However, at the low-metallicity end, the distinction between accreted and *in situ* populations is blurred; (iv) regarding the status of GCs whose origin is ambiguous, we conclude the following: the position in Si–Fe plane suggests an *in situ* origin for Liller 1 and a likely accreted origin for NGC 5904 and NGC 6388. The case of NGC 288 is unclear, as its orbital properties suggest an accretion origin, its chemical composition suggests it may have formed *in situ*.

Key words: Galaxy: formation – Globular Clusters; Galaxy: evolution.

1 INTRODUCTION

In a lambda cold dark matter cosmology, galaxies grow in mass due to the process of hierarchical assembly, whereby low-mass structures merge together to form the galaxies we observe in the local Universe. The signature of this process can be identified in the Milky Way, in the form of halo stellar streams (e.g. Helmi et al. 1999; Belokurov et al. 2006; Ibata, Lewis & Martin 2016), substructure in phase space, such as the *Gaia*-Enceladus/Sausage system (GE/S, Belokurov et al. 2018; Haywood et al. 2018; Helmi et al. 2018; Mackereth et al. 2019), and ongoing accretion, such as

the Sagittarius dwarf spheroidal (Sgr dSph, Ibata, Gilmore & Irwin 1994).

The satellites involved in such merger events naturally brought with them a cohort of globular clusters (GCs, e.g. Peñarrubia, Walker & Gilmore 2009), which survived the tidal interaction with the central halo and today are an integral part of the Galactic GC system. For decades, this has been the focus of various studies (e.g. Searle & Zinn 1978; Fall & Rees 1985; Ashman & Zepf 1992; Brodie & Strader 2006), aiming at using age, chemical composition, and phase-space information in order to, on one hand, understand the origin of the Galactic GC system, and on the other constrain the early history of mass assembly of the Milky Way. Key to that enterprise is to discern which of the Galactic GCs were formed *in situ* and which were accreted. In the last decade, the

* E-mail: d.hortadarrington@2018.ljmu.ac.uk

availability of precise ages (Marín-Franch et al. 2009; VandenBerg et al. 2013) has led to the discovery of the bifurcation in the age–metallicity relation of Galactic GCs (Marín-Franch et al. 2009; Forbes & Bridges 2010; Leaman, VandenBerg & Mendel 2013), which, combined with results from high-resolution hydrodynamical cosmological simulations of Milky Way analogues, has further constrained the origin the Galactic GC system (Kruijssen et al. 2019; Myeong et al. 2019). Furthermore, the advent of the *Gaia* survey (Gaia Collaboration 2018), and the resulting precise 6D phase-space information have made possible a much better characterization of the properties of the Galactic GC system.

Along those lines, a recent study by Massari, Koppelman & Helmi (2019) presented a new classification of the Galactic GC system in terms of the kinematic properties of its members. By studying their distribution in integral of motions (hereafter, IOM) space, Massari et al. (2019) established an association of each GC to one of the following main groups: main disc (MD), main bulge (MB), *Gaia*-Enceladus (GE), Sagittarius (Sag), Helmi streams (H99), Sequoia (Seq), low energy (LE), and high energy (HE).

The 16th data release of the Sloan Digital Sky Survey (DR16 Ahumada et al. 2019) includes data for over 450k stars from the APOGEE survey (Majewski et al. 2017), placing us in an advantageous position to obtain detailed chemical-abundance information for stars that are members of a significant fraction of the total Galactic GC population (Mészáros et al. 2015; Schiavon et al. 2017b; Mészáros et al. 2018; Masseron et al. 2019; Nataf et al. 2019). Such data will substantially further our understanding of the origin of the Galactic GC system, and in the process will help constrain the assembly history of the Milky Way. In this paper, we present an examination of the chemical properties of the GC groups identified by Massari et al. (2019). Our goal is to check whether subgroups that are defined purely on the basis of orbital properties can also be distinguished in terms of their chemical properties. In the process it is also possible to verify whether the chemical compositions are consistent with the star formation and chemical enrichment histories expected from the systems they are associated with.

This paper is structured as follows. In Section 2, we briefly describe our data. In Section 3, we describe the sample used and the criteria adopted to define GC membership, and in Section 4, we present the results obtained from the examination of the chemical properties of the kinematically defined GC groups. Section 5 summarizes our results and conclusions.

2 DATA

We use data from the 16th data release of SDSS-IV (Ahumada et al. 2019), which contains refined elemental abundances (Jönsson et al. 2019, submitted) from the APOGEE-2 survey (Majewski et al. 2017), which is one of four SDSS-IV (Blanton et al. 2017) experiments. APOGEE-2 is a near-infrared high signal-to-noise ratio (S/N > 100 pixel^{-1}), high-resolution ($R \sim 22\,500$) spectroscopic survey of over 450 000 Milky Way stars in the near-infrared *H* band (1.5–1.7 µm). Observations were based on two twin NIR spectrographs (Wilson et al. 2019) attached to the 2.5 m telescopes at Apache Point (Gunn et al. 2006), and Las Campanas Observatories. Targets were selected in general from the 2MASS point-source catalogue, employing a dereddened $(J - Ks) \geq 0.3$ colour cut in up to three apparent *H* magnitude bins. Reddening corrections were determined using the Rayleigh–Jeans Colour Excess method (RJCE; Majewski, Zasowski & Nidever 2011), based on NIR photometry from the 2MASS point source catalogue (Skrutskie et al. 2006), and mid-IR

data from the *Spitzer*-IRAC GLIMPSE-I,-II, and -3D (Churchwell et al. 2009) when available from *WISE* (Wright et al. 2010). A more in-depth description of the APOGEE survey, target selection, raw data, data reduction, and spectral analysis pipelines can be found in Majewski et al. (2017), Holtzman et al. (2015), Nidever et al. (2015), García Pérez et al. (2016), Jönsson et al. (2018), Zasowski et al. (2017), respectively. All the APOGEE data products used in this paper are those output by the standard data reduction and analysis pipeline. The data are first processed (Nidever et al. 2015; Jönsson et al. in preparation) before being fed into the APOGEE stellar parameters and chemical-abundances pipeline (ASPCAP; García Pérez et al. 2016; Jönsson et al. in preparation). ASPCAP makes use of a specifically computed spectral library (Zamora et al. 2015; Holtzman et al. 2018; Jönsson et al. in preparation), calculated using a customized *H*-band line-list (Shetrone et al. 2015; Cunha et al. in preparation), from which the outputs are analysed, calibrated, and tabulated (Holtzman et al. 2018).

3 GLOBULAR CLUSTER SAMPLE AND MEMBERSHIP

3.1 Main sample

In this subsection, we describe the method employed for determining the GC sample in APOGEE DR16. We build on previous work that has derived a GC sample in earlier data releases of APOGEE (Mészáros et al. 2015; Schiavon et al. 2017b; Nataf et al. 2019) and use the GC catalogues from Harris (1996), Baumgardt & Hilker (2018), and Baumgardt et al. (2019) in order to establish GC membership of stars in the DR16 sample. The methodology employed for identifying GC members is two-fold: the first step comprises the determination of an initial sample based on the values from the aforementioned catalogues. For this, we make use of data on GC positions (Galactic latitude and longitude), radial velocities, the radial velocity dispersions, tidal radii, and mean metallicity values.

We use these values, and the values provided by APOGEE DR16 catalogue, to associate any star to be a member of a GC if

(i) $\left| \, [\mathrm{Fe/H}]_\star - \langle[\mathrm{Fe/H}]_\mathrm{GC}\rangle \, \right| \leq 0.5$
(ii) $\left| \, rv_\star - \langle rv_\mathrm{GC}\rangle \, \right| \leq 2\,\sigma_\mathrm{GC}$
(iii) $d_\mathrm{proj} \leq 2\,r_\mathrm{vir}$

where [Fe/H] is the iron abundance, $rv_\star$ is the stellar heliocentric radial velocity, σ_GC is the cluster's radial velocity dispersion, d_proj is the projected distance between the star and the GC centre, and r_vir is the cluster's tidal radius. For GCs which are known to present a spread in metallicity (namely, NGC 6715, Terzan 5, and ω Cen), criterion (i) was omitted.

The GC iron abundances and centre coordinates were extracted from the 2010 edition of the Harris catalogue (Harris 1996), whereas the GC radial velocities, velocity dispersions, and tidal radii were obtained from the latest versions of the Baumgardt & Hilker catalogue,[1,2] (Baumgardt & Hilker 2018; Baumgardt et al. 2019). The stellar data come from APOGEE.

The first step of the procedure consisted of the application of criteria (i) to (iii) above, which yielded a preliminary sample of ~3650 stars. Having obtained this preliminary sample, the second step involved examining the metallicity distribution functions (MDFs)
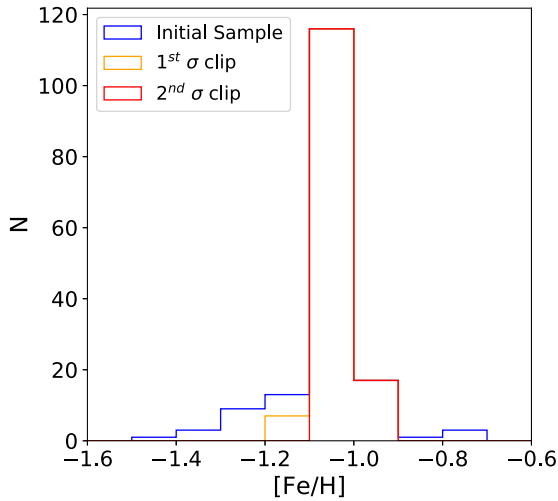
Figure 1. Example of the σ-clipping method employed to determine GC candidate members from our initial sample. The mean metallicity value from the Harris catalogue for NGC 6121 is [Fe/H] = −1.16, which lies very close to the peak of the distribution of our sample.

of the candidates selected in the first pass, which adopted a very broad [Fe/H] search interval. If the MDF peaked at a value within 0.3 dex from the Harris catalogue value, and the distribution did not present tails of more than 0.3 dex away from the mean [Fe/H] value, all candidates were deemed GC members. For those cases in which the MDF peaked within 0.3 dex of the Harris catalogue value, but presented a broader, less peaked, distribution, the sample was further cleaned through σ-clipping, as follows. We computed the mean and standard deviation of the [Fe/H] values, and then conducted the σ-clipping procedure by removing any member candidates that presented [Fe/H] abundances 1σ away from the mean. However, for most GCs the resulting clipped MDF still presented tails in the distribution, so we had to perform a second σ clipping, removing stars that deviated from the mean [Fe/H] value by more than two times the newly computed σ value. Fig. 1 illustrates the σ-clipping method employed and how successfully it works in defining GC candidate members from our initial sample, removing any false positives. For a full visualization of all the MDF cuts performed on the 43 GCs in our final main GC sample and the resulting radial velocity distribution, see Appendix A. We found that, by conducting this methodology, we were able to minimize false positives and obtain a reliable sample of GC members in APOGEE DR16. For 11 GCs from our original sample, fewer than 3 star members could be identified, so these GCs were removed from consideration. The final sample contained 3090 stars, associated with 46 GCs. Our selection procedure is quite conservative and likely excludes GC members. However, sample purity is more important for our goals than completeness. The mean elemental abundances, *rv* values, and associated standard deviations for the member stars for each GC are listed in Table 1. For GCs with large [Fe/H] spreads (namely, ω Cen, NGC 6715, and Terzan 5), mean abundances are not entirely meaningful. Moreover, in such cases the mean abundance ratios do not necessarily reflect those of the environments the GCs were born. Therefore, we removed these clusters from consideration. With this additional cut, our final working sample contains 1728 stars associated with 43 GCs.

Recently, Mészáros et al. (2019) performed a careful GC membership analysis, obtaining a sample that is very similar to ours. They proceeded to study star-to-star internal abundance variations

in GCs, with data based on the BACCHUS (Masseron, Merle & Hawkins 2016) abundance pipeline. We have repeated our entire analysis adopting both (Mészáros et al. 2019) member sample and abundances and obtained the same results as presented in this paper.

3.2 Globular cluster groups

In this subsection, we briefly discuss how the GCs in our sample are distributed across the kinematic groups defined by Massari et al. (2019) (see Fig. 2). From our main sample of 43 GCs, we find that 9 can be associated with the MD group, 10 to the MB, 9 to the GE dwarf spheroidal, 5 to the H99, 6 to the LE group, and 1 to the Seq dwarf spheroidal. An additional five GCs from our sample could not be unambiguously associated with a single group by Massari et al. (2019). The GC NGC 3201 could be associated with either of the GE or Seq group, NGC 5904 could belong to either GE or H99, and Liller 1 is listed as unclassified. Similarly, NGC 6388 is originally classified as an MB GC by (Massari et al. 2019). However, recent work has shown that NGC 6388 can be associated with the Sequoia accretion event based on its eccentric-retrograde orbit (Myeong et al. 2019). For this work, we initially follow the Massari et al. (2019) classification and include NGC 6388 in the MB subgroup, and study its chemical-abundances in order to discern if this GC is from *in situ* or accreted origin. Along the same lines, since it has recently been shown that NGC 3201 could be associated kinematically to the Sequoia dwarf remnant (Myeong et al. 2019), we choose to include these GCs in the Seq group. The remaining two GCs for which Massari et al. (2019) do not find a clear subgroup association (namely, NGC 5904 and Liller 1) are initially marked as unclassified and are discussed in Section 4.3. For the final list of the GCs obtained in the main sample and the kinematic group association see Table 3.

3.3 Elemental abundances and orbital parameters

In this paper, we report an examination of the APOGEE DR16 chemical-compositions for GCs from various subgroups. Specifically, we focus on studying trends in α-element abundances as a function of [Fe/H] to gain insights into the nature of the subgroups. Our goal is to examine how the kinematic classification by Massari et al. (2019) maps into chemical composition space. In so doing we expect to constrain the nature of the progenitors of the various subsystems making up the Galactic halo, given the relation between chemical compositions stellar populations and their histories of star formation and chemical enrichment. This also makes possible a more clear distinction between GCs formed *in situ* from those belonging to accreted systems

We focus on calibrated abundances (Jönsson et al. 2018), which have been compared in detail with independent determinations by other groups. Of relevance to this work, Jönsson et al. (2018) show that Si abundances, although differing from those of some of the other groups by statistically significant zero-point shifts, show no trends with stellar parameters. Since our results depend fundamentally on relative differences between abundances from a homogeneous set, such small zero-point effects are not important. The α-element of choice for this study is silicon. We use the [Si/Fe] abundances, as silicon has been shown in previous data releases to be one of the most reliable α-abundance measurements in APOGEE (Jönsson et al. 2018). Magnesium is another α-element for which APOGEE provides exquisite abundances, however it is affected by internal GC evolution (e.g. Bastian & Lardo 2018), so we remove it

Table 1. From left to right, GC name, mean [Fe/H], mean [Si/Fe], and mean radial velocity obtained for the final list of GCs in the main GC sample from APOGEE DR16.

| Name	$\langle$[Fe/H]$\rangle$	$\langle$[Si/Fe]$\rangle$	$\langle V_{los} \rangle$	Name	$\langle$[Fe/H]$\rangle$	$\langle$[Si/Fe]$\rangle$	$\langle V_{los} \rangle$
NGC 104	-0.72 ± 0.04	0.23 ± 0.04	-18.8 ± 7.3	NGC 6397	-2.02 ± 0.04	0.3 ± 0.06	19.5 ± 2.8
NGC 288	-1.26 ± 0.04	0.29 ± 0.03	-44.5 ± 2.2	NGC 6441	-0.39 ± 0.12	0.13 ± 0.13	10.8 ± 15.3
NGC 362	-1.09 ± 0.04	0.13 ± 0.04	223.6 ± 5.3	NGC 6522	-1.04 ± 0.06	0.22 ± 0.10	-12.8 ± 7.6
NGC 1851	-1.07 ± 0.04	0.14 ± 0.05	320.7 ± 5.9	NGC 6539	-0.39 ± 0.09	0.2 ± 0.07	33.8 ± 4.4
NGC 1904	-1.5 ± 0.07	0.15 ± 0.04	207.4 ± 2.6	NGC 6540	-1.01 ± 0.03	0.21 ± 0.04	-14.4 ± 1.1
NGC 2808	-1.04 ± 0.06	0.15 ± 0.06	103.4 ± 8.4	NGC 6544	-1.44 ± 0.05	0.22 ± 0.04	-38.6 ± 4.6
NGC 3201	-1.35 ± 0.05	0.16 ± 0.04	495.4 ± 3.3	NGC 6553	-0.16 ± 0.1	0.09 ± 0.07	0.2 ± 9.5
NGC 4590	-2.24 ± 0.07	0.33 ± 0.05	-94.0 ± 3.2	NGC 6656	-1.69 ± 0.05	0.29 ± 0.11	-146.6 ± 5.6
NGC 5024	-1.92 ± 0.04	0.25 ± 0.08	-60.8 ± 3.4	NGC 6715	–	–	–
NGC 5053	-2.15 ± 0.15	0.38 ± 0.09	42.9 ± 1.3	NGC 6723	-1.0 ± 0.06	0.25 ± 0.03	-93.5 ± 3.4
ω Cen	–	–	–	NGC 6752	-1.47 ± 0.03	0.25 ± 0.05	-26.3 ± 4.7
NGC 5272	-1.4 ± 0.06	0.17 ± 0.07	-146.2 ± 4.1	NGC 6760	-0.71 ± 0.1	0.19 ± 0.05	-1.5 ± 5.8
NGC 5466	-1.78 ± 0.06	0.19 ± 0.12	108.1 ± 1.0	NGC 6809	-1.75 ± 0.04	0.23 ± 0.05	176.1 ± 3.6
NGC 5904	-1.19 ± 0.05	0.18 ± 0.05	53.8 ± 4.9	NGC 6838	-0.73 ± 0.04	0.22 ± 0.03	-22.7 ± 2.1
NGC 6121	-1.04 ± 0.03	0.34 ± 0.04	70.9 ± 3.4	NGC 7078	-2.28 ± 0.05	0.31 ± 0.07	-104.3 ± 5.2
NGC 6171	-0.97 ± 0.06	0.32 ± 0.08	-33.8 ± 3.1	NGC 7089	-1.46 ± 0.06	0.19 ± 0.07	-3.6 ± 5.5
NGC 6205	-1.46 ± 0.04	0.21 ± 0.07	-246.3 ± 5.2	Terzan 2	-0.82 ± 0.05	0.26 ± 0.02	133.2 ± 1.4
NGC 6218	-1.26 ± 0.03	0.26 ± 0.05	-40.7 ± 3.1	Terzan 5	–	–	–
NGC 6229	-1.25 ± 0.05	0.19 ± 0.06	-137.8 ± 2.7	Pal 5	-1.24 ± 0.02	0.11 ± 0.04	-58.9 ± 0.5
NGC 6254	-1.49 ± 0.04	0.27 ± 0.05	75.8 ± 3.9	Pal 6	-0.81 ± 0.09	0.28 ± 0.07	172.9 ± 2.3
NGC 6341	-2.22 ± 0.03	0.31 ± 0.07	-118.2 ± 6.7	Pal 10	0.09 ± 0.06	0.0 ± 0.01	-32.7 ± 4.9
NGC 6380	-0.72 ± 0.05	0.21 ± 0.02	-1.8 ± 7.8	Liller 1	-0.03 ± 0.05	0.01 ± 0.05	61.8 ± 3.5
NGC 6388	-0.54 ± 0.06	-0.03 ± 0.1	80.1 ± 10.5	HP 1	-1.14 ± 0.07	0.22 ± 0.06	40.9 ± 4.8

Table 2. From left to right, GC name, mean orbital energy, and mean angular momentum obtained for the final list of GCs in the main GC sample from APOGEE DR16 using the MWPotential2014 (Bovy 2015). There is no 6D phase-space information for Liller 1 provided in Vasiliev (2019), thus we are unable to obtain IOM for this GC.

Name	E (km^2 s^{-2})	L_Z (10^3 kpc $*$ km s^{-1})	Name	E (km^2 s^{-2})	L_Z (10^3 kpc $*$ km s^{-1})
NGC 104	-50892^{+74}_{-94}	$0.62^{+0.01}_{-0.01}$	NGC 6397	-66705^{+193}_{-190}	$0.33^{+0.01}_{-0.01}$
NGC 288	-41116^{+1125}_{-947}	$-0.34^{+0.03}_{-0.03}$	NGC 6441	-93869^{+2812}_{-3479}	$0.21^{+0.03}_{-0.03}$
NGC 362	-41406^{+1436}_{-1391}	$-0.07^{+0.01}_{-0.01}$	NGC 6522	-129873^{+1043}_{-737}	$0.01^{+0.01}_{-0.01}$
NGC 1851	-21934^{+537}_{-521}	$-0.22^{+0.02}_{-0.04}$	NGC 6539	-88145^{+1367}_{-1378}	$-0.18^{+0.00}_{-0.00}$
NGC 1904	-26641^{+655}_{-650}	$-0.17^{+0.05}_{-0.04}$	NGC 6540	-108006^{+1814}_{-2001}	$0.18^{+0.01}_{-0.01}$
NGC 2808	-39859^{+541}_{-690}	$0.13^{+0.01}_{-0.01}$	NGC 6544	-85401^{+474}_{-386}	$-0.07^{+0.02}_{-0.02}$
NGC 3201	6964^{+1307}_{-1402}	$-1.65^{+0.02}_{-0.02}$	NGC 6553	-101735^{+2577}_{-1883}	$0.25^{+0.02}_{-0.02}$
NGC 4590	-1010^{+1311}_{-801}	$1.27^{+0.02}_{-0.01}$	NGC 6656	-49027^{+204}_{-294}	$0.47^{+0.01}_{-0.01}$
NGC 5024	-14407^{+851}_{-861}	$0.33^{+0.01}_{-0.02}$	NGC 6715	22391^{+3784}_{-3525}	$0.79^{+0.01}_{-0.01}$
NGC 5053	-18934^{+925}_{-645}	$0.29^{+0.02}_{-0.02}$	NGC 6723	-85738^{+958}_{-1010}	$-0.02^{+0.01}_{-0.01}$
ω Cen	-66584^{+413}_{-271}	$-0.35^{+0.01}_{-0.01}$	NGC 6752	-69155^{+484}_{-522}	$0.41^{+0.01}_{-0.01}$
NGC 5272	-26985^{+454}_{-549}	$0.42^{+0.01}_{-0.01}$	NGC 6760	-78723^{+322}_{-265}	$0.34^{+0.01}_{-0.01}$
NGC 5466	18295^{+2946}_{-3170}	$-0.54^{+0.04}_{-0.04}$	NGC 6809	-69856^{+220}_{-212}	$0.09^{+0.01}_{-0.01}$
NGC 5904	-4945^{+2821}_{-2685}	$0.16^{+0.01}_{-0.01}$	NGC 6838	-56897^{+99}_{-92}	$0.67^{+0.00}_{-0.00}$
NGC 6121	-78561^{+289}_{-377}	$-0.07^{+0.02}_{-0.02}$	NGC 7078	-44942^{+811}_{-912}	$0.55^{+0.02}_{-0.02}$
NGC 6171	-93415^{+343}_{-259}	$0.06^{+0.01}_{-0.01}$	NGC 7089	-24793^{+1316}_{-1645}	$-0.15^{+0.04}_{-0.03}$
NGC 6205	-55754^{+314}_{-363}	$-0.2^{+0.01}_{-0.01}$	Terzan 2	-142240^{+1564}_{-1992}	$-0.04^{+0.00}_{-0.00}$
NGC 6218	-9536^{+878}_{-819}	$0.06^{+0.11}_{-0.13}$	Terzan 5	-139676^{+2229}_{-2447}	$-0.02^{+0.01}_{-0.01}$
NGC 6229	-77618^{+518}_{-442}	$0.24^{+0.01}_{-0.01}$	Pal 5	-9666^{+3131}_{-2722}	$0.88^{+0.08}_{-0.08}$
NGC 6254	-76969^{+692}_{-537}	$0.25^{+0.01}_{-0.01}$	Pal 6	-96285^{+1413}_{-1744}	$-0.01^{+0.00}_{-0.01}$
NGC 6341	-49372^{+809}_{-728}	$-0.05^{+0.01}_{-0.01}$	Pal 10	-59725^{+733}_{-648}	$0.6^{0.01}_{-0.01}$
NGC 6380	-105529^{+3090}_{-2754}	$-0.02^{+0.01}_{-0.01}$	Liller 1	–	–
NGC 6388	-101561^{+1853}_{-1486}	$-0.13^{+0.01}_{-0.01}$	HP 1	-114308^{+5219}_{-3012}	$-0.01^{+0.01}_{-0.01}$

Table 3. GCs obtained in APOGEE DR16 associated with the kinematic subgroups as defined in Massari et al. (2019), after removing GCs with less than 3 star members. The GCs highlighted in bold are associations that are uncertain. The number of APOGEE member stars associated with each GC are given in parentheses.

Kinematic group	Associated GCs
Main disc	NGC 7078(30), NGC 6760(11), NGC 6838(37), NGC 6218(62), NGC 6397(46), NGC 6752(97), NGC 104(176), NGC 6656(35), Pal 10(3)
Main bulge	NGC 6539(6), NGC 6171(51), Terzan 2(4), NGC 6553(23), NGC 6380(15), NGC 6522(6), **NGC 6388(24)**, NGC 6540(4), NGC 6723(7), HP 1(12)
Gaia-Enceladus	NGC 1904(17), NGC 2808(66), NGC 6205(80), NGC 6229(6), NGC 6341(10), NGC 362(49), NGC 7089(26), NGC 1851(30), NGC 288(35), **NGC 5904(167)**
Sequoia	NGC 5466(7), NGC 3201(114), **NGC 6388(24)**
Sagittarius	–
Helmi streams	NGC 5024(18), NGC 5053(11), NGC 4590(13), NGC 5272(110), Pal 5(3), **NGC 5904(167)**
Low energy	NGC 6809(60), Pal 6(5), NGC 6441(28), NGC 6121(140), NGC 6254(59), NGC 6544(21)
High energy	–
XXX	**Liller 1(4)**
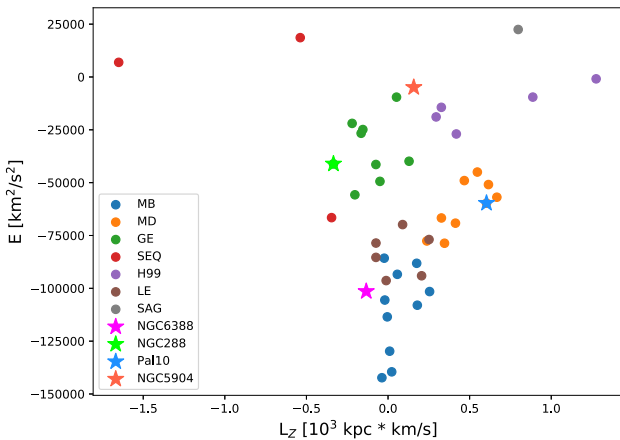
Figure 2. Orbital energy and vertical action as a function of orbital azimuthal action for the 46 GCs obtained in our initial main sample, divided into the kinematic associations identified by Massari et al. (2019).

from consideration when using the main sample. In order to verify that our choice of α-element does not affect our conclusions, we performed the analysis adopting [Mg/Fe] from first population stars and found that our results are unchanged. In addition, we compared our mean [Si/Fe] with those from the compilation by Pritzl, Venn & Irwin (2005), finding our values to be slightly lower, of the order of ~0.1 dex. Again, such a small zero-point difference has no impact on our results.

Orbital parameters were estimated for our sample of GCs as follows. We calculated the action integrals for each of the 46 GCs using the potential defined by Bovy (2015, MWPotential2014), using the publicly available code GALPY[3] (Bovy 2015; Mackereth & Bovy 2018). In order to obtain reliable kinematic measurements, we draw 100 samples for each of the 6D phase-space parameters given by the GC table in Vasiliev (2019), and obtain 100 estimates of the orbital parameters for each cluster, for which we then take the me-

dian and standard deviation as our value and associated uncertainty. Fig. 2 displays the energy (E) values obtained using this method as a function of the azimuthal action (L_Z) for all the GCs in our main sample, colour-coded by subgroup association. Highlighted as star symbols are GCs which display peculiar [Si/Fe] when compared to the remaining GCs in the same subgroup. We find that our orbital energy values differ from those of Massari et al. (2019). Such differences can be traced back to the adoption of different Galactic potentials with different total masses – while Massari et al. (2019) adopted a McMillan potential (McMillan 2017), the one adopted in this work was MWPotential2014 (Bovy 2015). We assessed the impact of Galactic potential choice on our results by re-running the calculations using the McMillan potential, and found that the GC associations to the various subgroups were unchanged, and are consistent with those found in Massari et al. (2019).

4 RESULTS

4.1 Disc, bulge, and low-energy GCs

In Fig. 3, we show the mean [Si/Fe] chemical-abundance measurements as a function of [Fe/H] for the MD (blue symbols), MB (orange symbols) and LE (red symbols) kinematically identified subgroups. Also plotted are the data for the GC Liller 1 (yellow dot), which is discussed in Section 4.3. At first glance the three subgroups occupy roughly the same locus in [Si/Fe] space, resembling the region of abundance space occupied by field stars from the disc and bulge components of the Milky Way (e.g. Hayden et al. 2015). Within the errors, the MD population displays a low-metallicity [Si/Fe] plateau until reaching [Fe/H] abundance values of approximately [Fe/H] $\simeq -0.6$, for which according to the Milky Way's Disc field population, we would expect a knee towards lower [Si/Fe] values (Alves-Brito et al. 2010). When considered in aggregate, the three subgroups display a clear knee at about [Fe/H] ~ -0.8, with a plateau at [Si/Fe] $\sim +0.25$ at lower metallicities and a trend of decreasing [Si/Fe] for increasing [Fe/H] at [Fe/H] $\gtrsim -0.8$, which mimics the behaviour of field stars. One GC deviates clearly from this trend, namely NGC 6388, with very low
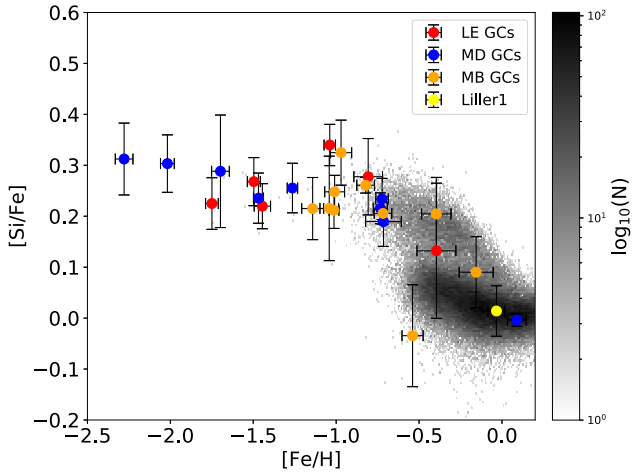
Figure 3. Mean [Si/Fe] versus [Fe/H] chemical-abundances for the low energy (red), main bulge (orange), and main disc (blue) GC subgroups, illustrated alongside Liller 1 (yellow), with the 1σ spread represented in black error bars. In grey we show the Galactic disc and bulge field populations defined kinematically according to Massari et al. (2019). From these abundance plots, by accounting for the 1σ spread uncertainties, we find that the more [Fe/H] rich LE GCs, namely NGC 6121, NGC 6441, and Pal 6 can be categorized to be from *in situ* origin. The other three LE GCs still occupy the same locus as the MD/MB subgroups, however due to their low [Fe/H] abundances and position in the IOM space (Fig. 2), it is possible that these more metal-poor GCs could be from an accreted origin. Furthermore, we find that Liller 1 occupies the same locus as the *in situ* GCs, which coupled with its high [Fe/H] value can be classified as an MB GC.

[Si/Fe] ~ 0.0 at [Fe/H] ~ -0.5. We discuss this interesting GC separately in Section 4.4.

When the three subgroups are considered separately, however, the relatively small number of GCs in our sample prevents the unequivocal identification of a 'knee' in the Si–Fe plane for any of the subgroups in Fig. 3. In the case of the MB subgroup, the sample does not contain enough GCs at [Fe/H] $\lesssim -0.8$ to firmly establish the existence of a low-metallicity [Si/Fe] plateau. The LE subgroup straddles properly both [Fe/H] sides of the 'knee' and the GCs seem to follow the same trend as the field population, but the sample is too small for a solid conclusion. The sample for the MD subgroup covers a wide range in [Fe/H] towards the metal-poor side of the knee, but contains only one GC on the metal-rich end, whose position on the Si–Fe is consistent with the existence of a knee in that subgroup. Again, the sample is not large enough at [Fe/H] $\gtrsim -0.8$ for a robust conclusion. The GC on the metal-rich end of the MD subgroup is Pal 10. We checked to see whether the orbital properties of this cluster match those of the MD GC population. In Fig. 2, we show that Pal 10 does follow a disc-like orbit, displaying energy values of $E \sim -6000\,\mathrm{km^2\,s^{-2}}$ and following a prograde orbit (i.e. $L_Z \sim 0.7\,10^3\,\mathrm{kpc\,km\,s^{-1}}$), therefore it is likely to belong to the MD subgroup. All in all, the MB and MD subgroups follow the trend defined by the field population, thus we conclude that these subgroups share an *in situ* origin.

Since the origin of the LE subgroup is contentious, the locus of GCs from that subgroup merits some attention. Our results show that the GCs from this subgroup occupy the same locus in [Si/Fe] versus [Fe/H] space as the MD/MB GCs. This result is in line with the similarity of these subgroups in E–L_Z space, (see Fig. 2 of this paper and fig. 3 of Massari et al. 2019) We note, however, that at [Fe/H] $\lesssim -1.5$ it is almost impossible to distinguish between accreted and *in situ* GCs in the Si–Fe plane, so that an accreted

origin for the three most metal-poor GCs in the LE group (namely, NGC 6254, NGC 6544, and NGC 6809) cannot be ruled out.

In summary, from the point of view of kinematics, the low energy defining this subgroup makes it hard to distinguish it from the MD/MB subgroups (Fig. 2). On the basis of the chemistry, while the metal-rich GCs NGC 6441, Pal 6, and NGC 6121 are clearly associated with the MD/MB subgroups, the association of the more metal-poor GCs NGC 6254, NGC 6544, and NGC 6809 is more uncertain, given that accreted and *in situ* GCs occupy the same locus in the Si–Fe plane for those metallicities. We conclude that, while the overall trend on the Si–Fe plane of the LE GCs in our sample suggests an *in situ* origin, the position of that subgroup in IOM space does not preclude some of the members of that category having an accreted origin.

Finally, we highlight the case of NGC 6388. Although that GC is classified by Massari et al. (2019) as belonging to the MB subgroup, it is characterized by very low [Si/Fe] (~ -0.03), departing by $\sim 2\sigma$ from the mean [Si/Fe] of that subgroup at [Fe/H] ~ -0.5. We discuss this GC in more detail in Section 4.4.

4.2 Accreted subgroups

In this subsection, we examine the distribution of GCs of accreted origin in the Si–Fe plane. Our analysis focuses on the following subgroups: H99, GE, and Seq.

The data for these GCs are displayed in Fig. 4. We first focus on a comparison between the positions occupied by the accreted and *in situ* clusters. Our results show that the GCs associated with the three putative accreted systems all fall on the same locus in the [Si/Fe] plane, positioned on average at lower [Si/Fe] values than the MD and MB population (illustrated in Fig. 4 as grey points). This is commonly interpreted as the result of a history of star formation and chemical enrichment typical of low-mass galaxies, which differs from that of the Milky Way (e.g. Tolstoy, Hill & Tosi 2009). The accreted origin of the GCs that are kinematically associated with GE, H99, and Seq is further confirmed by the fact that their position in the [Si/Fe] plane mimics that of field populations linked with past accretion events (Hayes et al. 2018; Mackereth et al. 2019). We calculate the mean [Si/Fe] abundance given by GCs in the $-1.5 <$ [Fe/H] < -1 regime for both our accreted and *in situ* populations, and find that the accreted groups display on average [Si/Fe] $= +0.17 \pm 0.05$, whereas the *in situ* subgroups display a higher average abundance [Si/Fe] $= +0.25 \pm 0.03$. This means that the two distributions differ at the ~ 91.5 per cent level.

Having established that the accreted subgroups occupy a locus of lower [Si/Fe] than that of *in situ* populations, we now turn to a discussion of the relative positions of the GCs from the three accreted subgroups in the Si–Fe space. As pointed out above, the GCs associated with the GE, H99, and Seq subgroups occupy the same locus on the abundance plane, within the errors. Such similarity in chemical space can be understood in two possible ways. On one hand, the different accreted subgroups may be associated with three separate similar-mass satellites. Alternatively, some, or perhaps all of them, could be part of the same accreted satellite. Consideration of the kinematic properties of the three systems may help distinguish between these scenarios. The GE system is strongly bound and mildly retrograde, whereas the other two groups are slightly less bound, with Seq being strongly retrograde and H99 strongly prograde. Massari et al. (2019) argue that two of the GCs associated with the Sequoia system (namely, NGC 3201 and ω Cen) have a relatively high probability of belonging to GE. Moreover, they point out that the Sequoia system's position in IOM space
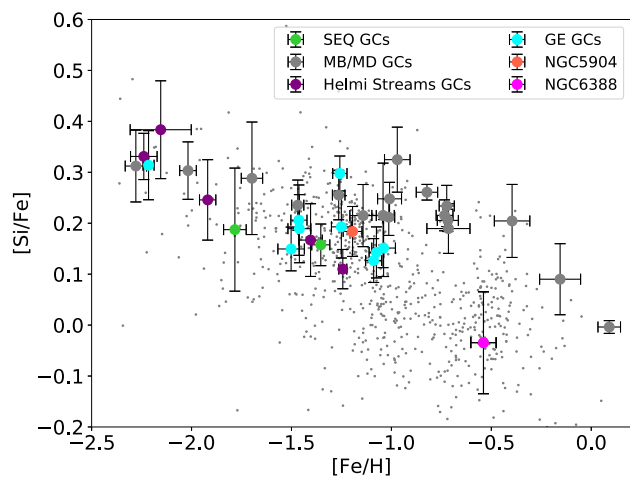
Figure 4. Mean [Si/Fe] versus [Fe/H] for the GE (cyan), Seq (green), H99 (purple), and MD/MB (grey) GC subgroups, illustrated alongside NGC 5904 (red) and NGC 6388 (magenta), with the 1σ spread represented in black error bars. In grey we show the halo field population defined as in Massari et al. (2019). The GE, Seq, and H99 accreted dwarf spheroidal subgroups occupy the same locus, displaying lower mean [Si/Fe] values to the GCs from the MD and MB populations at the same metallicity range $-1.5 <$ [Fe/H] < -1. According to galaxy chemical-evolution models, this suggests that either: both accreted dwarf spheroidals must have had a similar chemical-evolution history and therefore have been of similar mass, or that some, possibly all, originate from the same accretion event. Below [Fe/H] < -1.5, the *in situ* and accreted groups are indistinguishable in the Si–Fe plane. NGC 288 displays higher [Si/Fe] values than the rest of the GE subgroup GCs (∼0.15 dex greater) of similar metallicity, however displays a clear accreted-like orbit (see Fig. 2). NGC 5904 clearly occupies the same locus as the accreted population of GCs. However, due to the uncertainties in the measurements, it is impossible to suggest to which accreted subgroup NGC 5904 belongs to. Along the same lines, NGC 6388 occupies the same locus as the [Fe/H]-rich halo field population, which coupled with its retrograde orbit hints that this GC belongs to an accreted subgroup.

coincides with that of debris that Helmi et al. (2018) ascribe to *Gaia*-Enceladus.

Along the same lines, Massari et al. (2019) analysed the Helmi stream GCs employing the methodology described in Koppelman et al. (2019b), and found that, when accounting for the age uncertainties, H99 occupies a locus in age–metallicity space that is consistent with the *Gaia*-Enceladus and Sequoia GC subgroups. Moreover, it has been shown that the field populations of the *Gaia*-Enceladus, Sequoia, and Helmi stream occupy the same locus in [Mg/Fe] versus [Fe/H] and [Al/Fe] versus [Fe/H] planes (Koppelman et al. 2019a), and that the Helmi stream displays an MDF which peaks at a value of [Fe/H] ~ -1.5 (Koppelman et al. 2019b), similar to value at which the *Gaia*-Enceladus MDF peaks (Helmi et al. 2018; Mackereth et al. 2019).

We conclude that the combined evidence from GC subgroup chemistry and kinematics is suggestive of either a common origin for the Sequoia, Helmi stream, and *Gaia*-Enceladus stellar systems, or that these subgroups are associated with satellites which underwent similar chemical enrichment histories.

In closing this subsection we comment on the interesting case of NGC 288. On the basis of kinematics, Massari et al. (2019) assign it unambiguously to the GE subgroup, with a retrograde orbit and high orbital energy (see Fig. 2). However, its elemental abundances place it squarely on the *in situ* branch, $\sim 2\sigma$ off the mean of the GE subgroup at the same [Fe/H]. We checked to

see if this result survives when other α-elements are considered, and find that NGC 288 also displays [Mg/Fe] and [Ca/Fe] values $\sim 2\sigma$ away from the mean of the GE subgroup, with the GE subgroup presenting mean values of $\langle$[Mg/Fe]$\rangle_{GE} = +0.17 \pm 0.07$ and $\langle$[Ca/Fe]$\rangle_{GE} = +0.19 \pm 0.04$, respectively, and NGC 288 displaying [Mg/Fe]$_{NGC\,288} = +0.31 \pm 0.04$ and [Ca/Fe]$_{NGC\,288} = +0.26 \pm 0.09$, for the same [Fe/H]. It is difficult to reconcile the orbital and chemical properties of NGC 288, so we suggest that NGC 288 is likely an accreted GC with a peculiar chemical composition.

4.3 NGC 5904 and Liller 1

The study by Massari et al. (2019) did not assign Liller 1 to any particular kinematic subgroup, and concluded that NGC 5904 could be associated with either the GE or H99 subgroup. In this subsection, we examine these GCs' positions in chemical space to see whether that information can help clarify whether they have an accreted or *in situ* origin.

We first compare the [Si/Fe] versus [Fe/H] abundance measurements obtained for Liller 1 with the other identified subgroups (see Fig. 3). Our results show that within the uncertainties, Liller 1 occupies the same locus in the [Si/Fe] versus [Fe/H] abundance plane as the *in situ* population, and therefore belongs to either the MD or MB subgroup. Unfortunately, there is no 6D phase-space information for Liller 1 (see Vasiliev 2019, for details), and therefore we are unable to place kinematic constrains on the origin of this GC. Furthermore, Liller 1 is quite metal rich, with a mean value of $\langle$[Fe/H]$\rangle_{Liller\,1} \simeq -0.03 \pm -0.05$, which is much higher than the metallicities of the accreted GCs. Thus, our results suggest that Liller 1 has an *in situ* origin, agreeing with previous studies (e.g. Bica, Ortolani & Barbuy 2016).

In the case of NGC 5904, our results show that the mean abundances place it on the same locus as the GCs associated with the accreted subgroups. Therefore, within the uncertainties our results suggest that NGC 5904 has an accreted origin (agreeing with the suggestion by Massari et al. 2019). However, since it is impossible to distinguish the accreted groups in Si–Fe space, we cannot establish an association of NGC 5904 to any particular accreted subgroup.

4.4 NGC 6388

As pointed out in Section 4.1, NGC 6388 displays a very low [Si/Fe] abundance ratio, departing significantly from the locus of the MB subgroup, to which it was associated by Massari et al. (2019). Its position on the Si–Fe plane is consistent with an extrapolation towards high metallicity of the trend established by the accreted subgroups at [Fe/H] $\lesssim -1$. It also falls on top of the accreted field population in Fig. 4. The mean abundances for NGC 6388 are based on values for 24 members, which we consider to be statistically robust. Specifically, the mean silicon abundance of NGC 6388 members ($\langle$[Si/Fe]$\rangle = -0.03 \pm 0.1$) deviates from that of the high-α sequence at same [Fe/H] ($\langle$[Si/Fe]$\rangle_{high-\alpha} = +0.17 \pm 0.05$) by $\sim 2\sigma$. It is also lower than that of the low-α sequence ($\langle$[Si/Fe]$\rangle_{low-\alpha} = +0.02 \pm 0.04$) by $\sim 1\sigma$. We note, however, that Carretta & Bragaglia (2018) obtained abundances for a comparable sample of NGC 6388 members, obtaining ~ 0.4 dex higher mean [Si/Fe]. Wallerstein, Kovtyukh & Andrievsky (2007) also obtained a ~ 0.3 dex higher mean [Si/Fe], although their mean abundances of Ti and Ca were around solar or lower ($\sim +0.06$ and -0.05, respectively), depending on the log g adopted. On the other hand, Mészáros et al.

(2019) analysed the APOGEE spectra using a different pipeline, obtaining similar results to those presented in this paper.

In order to check whether our result is due to systematics in the [Si/Fe] abundance ratios of NGC 6388 stars, we examined the abundances of other α-elements, such as Mg and Ca. For the latter element we found $\langle[\text{Ca/Fe}]\rangle = +0.09 \pm 0.11$, which is lower than the values for the MB population at the same [Fe/H] ([Ca/Fe] $= +0.19 \pm 0.02$), deviating at the $\sim 1\sigma$ level. Before estimating mean [Mg/Fe], one needs to select GC members that are not affected by the multiple population phenomenon. In order to isolate NGC 6388 stars belonging to the so-called first population, we proceeded as follows. We use [N/Fe] in order to identify first population stars, since this abundance ratio is strongly enhanced in their second population counterparts (see e.g. Renzini et al. 2015; Schiavon et al. 2017a, b; Bastian & Lardo 2018). We define as first population stars those located within the bottom quartile of the [N/Fe] distribution of NGC 6388 members. By proceeding in this way, we are confident that we managed to isolate a subsample of first population GC stars, whose Mg abundances are not affected by the multiple populations phenomenon. For this subsample, we obtained $\langle[\text{Mg/Fe}]\rangle = +0.07 \pm 0.11$, which again is lower than the mean value for the MB population ($\langle[\text{Mg/Fe}]\rangle = +0.27 \pm 0.06$) by $\sim 2\sigma$.

It is worth noticing that the relative position of NGC 6388 in α-Fe space is not the same according to different α-elements. When Si is considered, NGC 6388 falls below the low-α sequence at the 1σ level. On the other hand, the cluster falls on top of the low-α sequence when Mg or Ca are considered.

Due to NGC 6388 being a bulge GC, positioned in a crowded and dense field, it is likely that our sample is contaminated by field stars, mainly in the GC foreground. To ensure our previous findings are robust, we minimize field contamination by considering only N-rich stars, which belong to the 'second-population' GC population stars. To obtain a clean sample of 'second population' stars, we select only stars located at the top quartile of the [N/Fe] distribution. For second-population NGC 6388 stars defined in that manner, we find an average of $\langle[\text{Si/Fe}]\rangle = -0.07 \pm 0.08$, which places NGC 6388 even further away from the *in situ* population. This solidifies our initial findings, and confirms that NGC 6388 displays lower [Si/Fe] abundances than those of other MB GCs of similar metallicity.

Myeong et al. (2019) studied the properties of NGC 6388 in detail, showing that, on one hand, it is consistent with an accreted origin on account of its kinematic properties, but on the other its combination of age and metallicity places it on top of the relation defined by the *in situ* GC population for those two parameters (see also Kruijssen et al. 2019). We determined the orbital energy and azimuthal action of NGC 6388 (see Fig. 2), finding its orbit to be retrograde, in agreement with Myeong et al. (2019), but cannot distinguish between a possible association to the MB, LE, or the Seq subgroups. Furthermore, Milone et al. (2019) classified NGC 6388 as a Type II GC, based on the ratio of first-population to second-population stars. They also obtain the IOM of this GC, and conclude that NGC 6388 is likely from an accreted origin.

We summarize our results for NGC 6388 as follows: (1) the [Si/Fe] abundance for this GC differs from that of the MB/MD population at the 2σ level; (2) it differs from that of the low-α at the 1σ level; (3) Fig. 4 shows that NGC 6388 falls on top of the accreted *field* halo populations in the Si–Fe plane; (4) its position in the IOM does not provide a unique distinction between an accreted or *in situ* origin. In view of these results, it is fair to conclude that the data suggest a possible accreted origin for NGC 6388.

5 CONCLUSIONS

In this work, we have employed the sixteenth data release from the SDSS/APOGEE survey in order to map the kinematic properties of Galactic GCs into their positions in the chemical compositions space. We contrast positions, and APOGEE abundances and radial velocities with information gathered from the 2010 edition of the Harris GC catalogue (Harris 1996) and the Baumgardt & Hilker GC catalogue (Baumgardt & Hilker 2018; Baumgardt et al. 2019) to obtain a primary GC sample in APOGEE, which we refine to obtain an accurate GC membership list. We obtain a final main GC sample of 3090 stars, associated with 46 GCs, from which then ω Cen, Terzan 5, and NGC 6715 are removed for reasons detailed in Section 3.1, leaving us with a sample of 1728 stars associated with 43 GCs. We assign membership to various kinematic subgroups according to the classification by Massari et al. (2019). We then examine the distributions of the various GC subgroups in chemical space, more specifically the plane defined by α and Fe abundances. After excluding GCs with fewer than three member stars, we identify in our sample 9 GCs associated with the MD group, 10 to the MB, 9 to the GE dwarf spheroidal, 5 to the H99, 6 to the LE group, 2 to the Seq dwarf spheroidal, and 0 to the Sag dwarf spheroidal. Furthermore, we find 2 GCs (namely, Liller 1 and NGC 5904) for which there remains an uncertain association.

We make use of Si abundance measurements in APOGEE as our tracer of α-elements abundance, and plot them as a function of [Fe/H] with the goal of gaining insight into the nature of the different kinematic subgroups. In this comparison, we search for any possible plateau or knees that may present themselves in an [α/Fe] versus [Fe/H] plane. Our results and conclusions are unchanged by adoption of the sample and abundances presented by Mészáros et al. (2019). Our conclusions can be summarized as follows:

(i) When considered together the *in situ* GC subgroups (main disc and main bulge, MD and MB) and the low-energy group (LE) follow the overall trend of the *in situ* populations (MB and MD) in chemical space, with a [Si/Fe] $\sim +0.25$ plateau at low metallicity and a change of slope (so-called knee) at [Fe/H] ~ -0.8.

(ii) GCs from accreted subgroups, namely *Gaia*-Enceladus (GE), Helmi streams (H99), and Sequoia (Seq) fall on the same area of chemical space as accreted field populations. This locus is characterized by [Si/Fe] $\lesssim +0.2$ at $-1.5 \lesssim$ [Fe/H] $\lesssim -1.0$, going down to solar or near sub-solar [Si/Fe] for [Fe/H] ~ -0.5. At [Fe/H] $\lesssim -1.5$, GCs from the accreted and *in situ* subgroups are indistinguishable in the Si–Fe plane.

(iii) When examined separately, the MD, MB, and LE subgroups track the field population, however due to the relatively small sample size these subgroups do not sample the metallicity space densely enough to define the trend separately from the other subgroups. Three out of six of the LE GCs (namely, NGC 6121, NGC 6441, and Pal 6) fall on the high-metallicity side of the knee and follow the trend of the field populations, leading to the conclusion that they have an *in situ* origin. The three metal-poor GCs from the LE subgroup (namely, NGC 6254, NGC 6544, and NGC 6809) fall in the region of Si–Fe where accreted and *in situ* GCs are indistinguishable, so their origin is less certain. We conclude that the chemical properties of the LE subgroup as a whole are consistent with an *in situ* origin, but given its borderline position in IOM space, individual clusters belonging to this subgroup could have an accreted origin.

(iv) GCs from the accreted H99 and GE subgroups occupy the same position in chemical space. That is also the case for the GCs in the Seq group, but since our sample contains only

two Seq GCs, the result for that subgroup is not as firm. This result suggests that GCs from these subgroups are associated with accreted satellites of similar masses, or possibly originating from one common progenitor. Based on its position on the IOM space, it is possible that the GCs from the Seq and GE subgroups actually once belonged to the same system, as suggested by other groups (e.g. Massari et al. 2019).

(v) NGC 6388 is found to present Si, Mg, and Ca abundances that are considerably lower than those of other GCs in the main bulge subgroup and similar [Fe/H]. The evidence from other studies in the literature is not conclusive, so more studies exploring other spectral regions and different α-elements are required to ascertain the low-α nature of this GC. Considering the orbital characteristics, a confirmation of this result will lend strong support to the notion that NGC 6388 was in fact accreted to the Milky Way, as also suggested by other groups (e.g. Milone et al. 2019; Myeong et al. 2019).

(vi) NGC 288 is found to present Si, Ca, and Mg abundances that are considerably higher than those of other accreted GCs of similar [Fe/H]. It is characterized by a highly unbound retrograde orbit. We conclude that NGC 288 is an unusual GC where the kinematic properties suggest an accreted origin which is not fully compatible with the its chemistry. More work is needed to clarify the origin of this object.

(vii) Comparison of the mean [Si/Fe] versus [Fe/H] chemical compositions of Liller 1 and NGC 5904 with those of the different kinematic subgroups suggests that Liller 1 possibly associated with the *in situ* subgroups and that NGC 5904 was likely accreted. We cannot, on the basis of the extant data, establish to which accreted subgroup this GC is associated.

In summary, the information provided by the sixteenth APOGEE data release has enabled a study of the chemical-abundances of the Galactic GC system, shedding light on the origin of a reasonably representative sample of the Milky Way GC system. The combination of the chemical-abundance information delivered by APOGEE and the kinematic 6D phase-space information provided by *Gaia* provides interesting insights into the origin of the Milky Way GCs. Expansion of such data bases to a larger sample of Galactic GCs will shed new light on the Galaxy's early mass assembly history.

REFERENCES

Ahumada R. et al., 2019, preprint (arXiv:1912.02905)
Alves-Brito A., Meléndez J., Asplund M., Ramírez I., Yong D., 2010, A&A, 513, A35
Ashman K. M., Zepf S. E., 1992, ApJ, 384, 50
Bastian N., Lardo C., 2018, ARA&A, 56, 83
Baumgardt H., Hilker M., 2018, MNRAS, 478, 1520
Baumgardt H., Hilker M., Sollima A., Bellini A., 2019, MNRAS, 482, 5138
Belokurov V. et al., 2006, ApJ, 642, L137
Belokurov V., Erkal D., Evans N. W., Koposov S. E., Deason A. J., 2018, MNRAS, 478, 611
Bica E., Ortolani S., Barbuy B., 2016, Publ. Astron. Soc. Aust., 33, e028
Blanton M. R. et al., 2017, AJ, 154, 28
Bovy J., 2015, ApJS, 216, 29
Brodie J. P., Strader J., 2006, ARA&A, 44, 193
Carretta E., Bragaglia A., 2018, A&A, 614, A109
Churchwell E. et al., 2009, PASP, 121, 213
Fall S. M., Rees M. J., 1985, ApJ, 298, 18
Forbes D. A., Bridges T., 2010, MNRAS, 404, 1203
Gaia Collaboration, 2018, A&A, 616, A1
García Pérez A. E. et al., 2016, AJ, 151, 144
Gunn J. E. et al., 2006, AJ, 131, 2332
Harris W. E., 1996, VizieR Online Data Catalog. p. VII/195
Hayden M. R. et al., 2015, ApJ, 808, 132
Hayes C. R. et al., 2018, ApJ, 852, 49
Haywood M., Di Matteo P., Lehnert M. D., Snaith O., Khoperskov S., Gómez A., 2018, ApJ, 863, 113
Helmi A., White S. D. M., de Zeeuw P. T., Zhao H., 1999, Nature, 402, 53

Helmi A., Babusiaux C., Koppelman H. H., Massari D., Veljanoski J., Brown A. G. A., 2018, Nature, 563, 85

Holtzman J. A. et al., 2015, AJ, 150, 148

Holtzman J. A. et al., 2018, AJ, 156, 125

Ibata R. A., Gilmore G., Irwin M. J., 1994, Nature, 370, 194

Ibata R. A., Lewis G. F., Martin N. F., 2016, AJ, 819, 13

Jönsson H. et al., 2018, AJ, 156, 126

Koppelman H. H., Helmi A., Massari D., Price-Whelan A. M., Starkenburg T. K., 2019a, A&A, 631, 6

Koppelman H. H., Helmi A., Massari D., Roelenga S., Bastian U., 2019b, A&A, 625, A5

Kruijssen J. M. D., Pfeffer J. L., Reina-Campos M., Crain R. A., Bastian N., 2019, MNRAS, 486, 3180

Leaman R., VandenBerg D. A., Mendel J. T., 2013, MNRAS, 436, 122

Mackereth J. T., Bovy J., 2018, PASP, 130, 114501

Mackereth J. T. et al., 2019, MNRAS, 482, 3426

McMillan P. J., 2017, MNRAS, 465, 76

Majewski S. R., Zasowski G., Nidever D. L., 2011, ApJ, 739, 25

Majewski S. R. et al., 2017, AJ, 154, 94

Marín-Franch A. et al., 2009, ApJ, 694, 1498

Massari D., Koppelman H. H., Helmi A., 2019, A&A, 630, L4

Masseron T., Merle T., Hawkins K., 2016, Astrophysics Source Code Library, record ascl:1605.004

Masseron T. et al., 2019, A&A, 622, A191

Mészáros S. et al., 2015, AJ, 149, 153

Mészáros S. et al., 2018, MNRAS, 475, 1633

Mészáros S., Wolosz J., 2020, MNRAS, 492, 1670

, Milone A. P., Marino, A. F., Da Costa, G. S. et al., 2019, MNRAS, 491, 531

Myeong G. C., Vasiliev E., Iorio G., Evans N. W., Belokurov V., 2019, MNRAS, 488, 1235

Nataf D. M. et al., 2019, AJ, 158, 14

Nidever D. L. et al., 2015, AJ, 150, 173

Peñarrubia J., Walker M. G., Gilmore G., 2009, MNRAS, 399, 1275

Pritzl B. J., Venn K. A., Irwin M., 2005, AJ, 130, 2140

Renzini A. et al., 2015, MNRAS, 454, 4197

Schiavon R. P. et al., 2017a, MNRAS, 465, 501

Schiavon R. P. et al., 2017b, MNRAS, 466, 1010

Searle L., Zinn R., 1978, ApJ, 225, 357

Shetrone M. et al., 2015, ApJS, 221, 24

Skrutskie M. F. et al., 2006, AJ, 131, 1163

Tolstoy E., Hill V., Tosi M., 2009, ARA&A, 47, 371

VandenBerg D. A., Brogaard K., Leaman R., Casagrand e L., 2013, ApJ, 775, 134

Vasiliev E., 2019, MNRAS, 484, 2832

Wallerstein G., Kovtyukh V. V., Andrievsky S. M., 2007, AJ, 133, 1373

Wilson J. C. et al., 2019, PASP, 131, 055001

Wright E. L. et al., 2010, AJ, 140, 1868

Zamora O. et al., 2015, AJ, 149, 181

Zasowski G. et al., 2017, AJ, 154, 198

APPENDIX A: GC METALLICITY AND RADIAL VELOCITY DISTRIBUTION FUNCTIONS
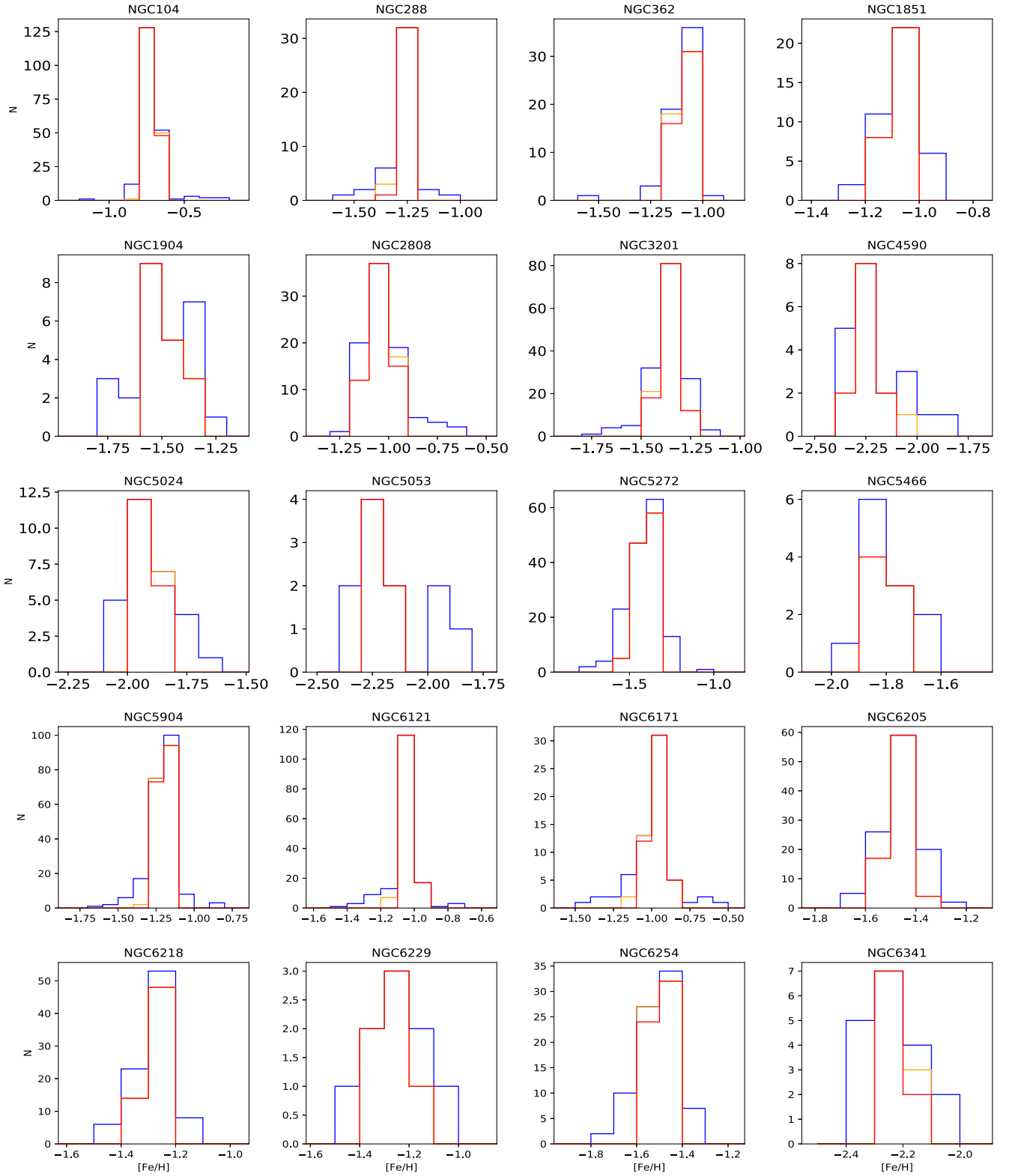
Figure A1. MDFs for the GCs in the main sample. The blue histogram represents the GC members obtained before employing the MDF sigma clip cut, for which the resulting members are highlighted as the yellow histogram. The red histogram are the resulting members after performing a second MDF sigma clip. Recall that for each GC a different clip was applied, depending on the cluster and the MDF distribution.
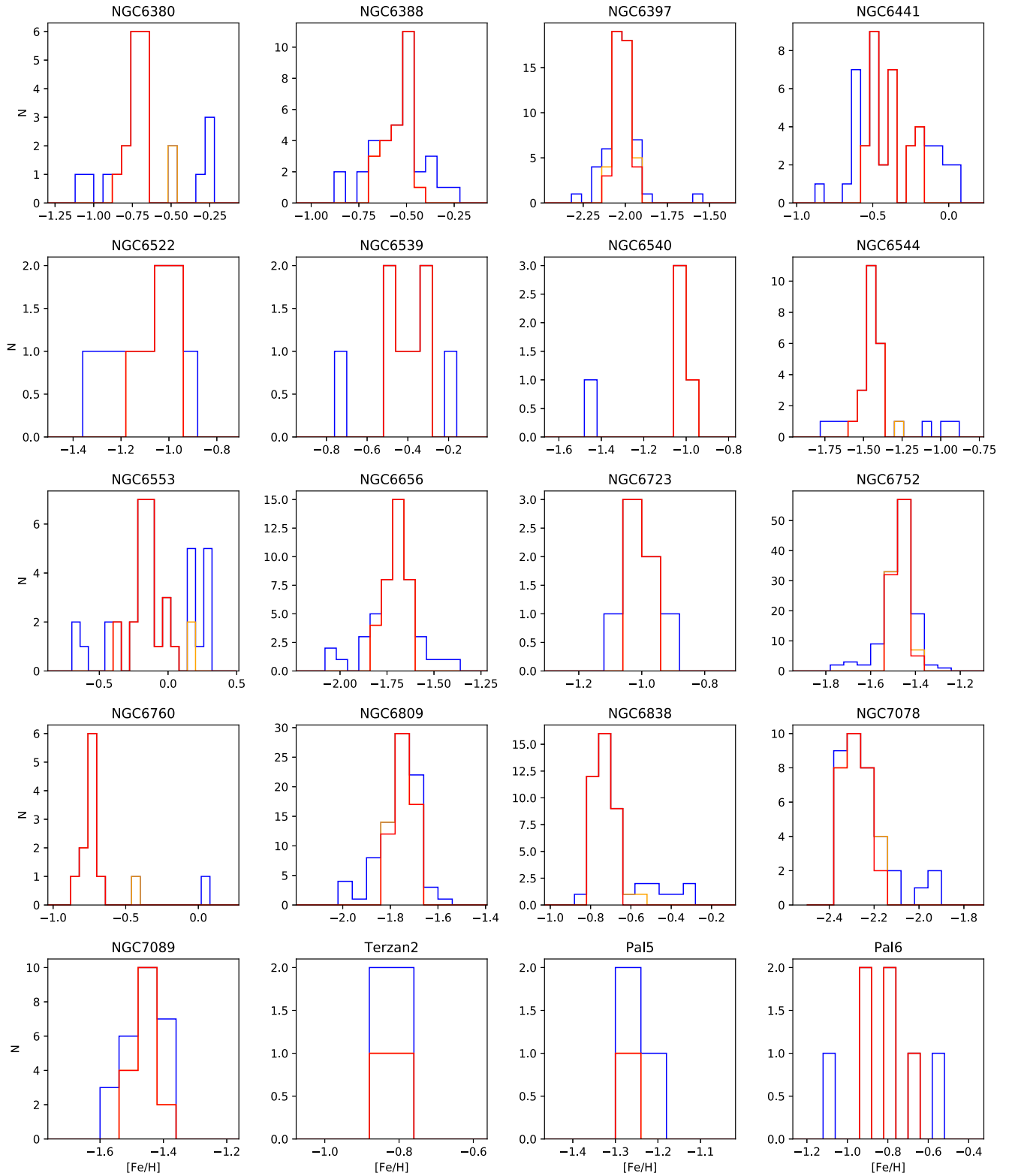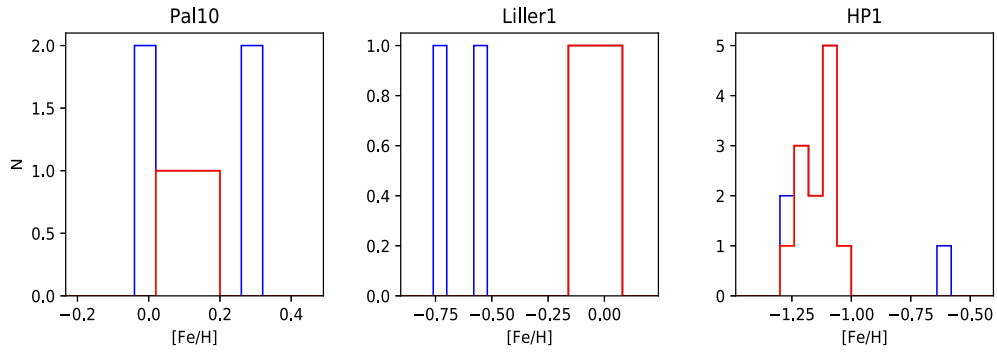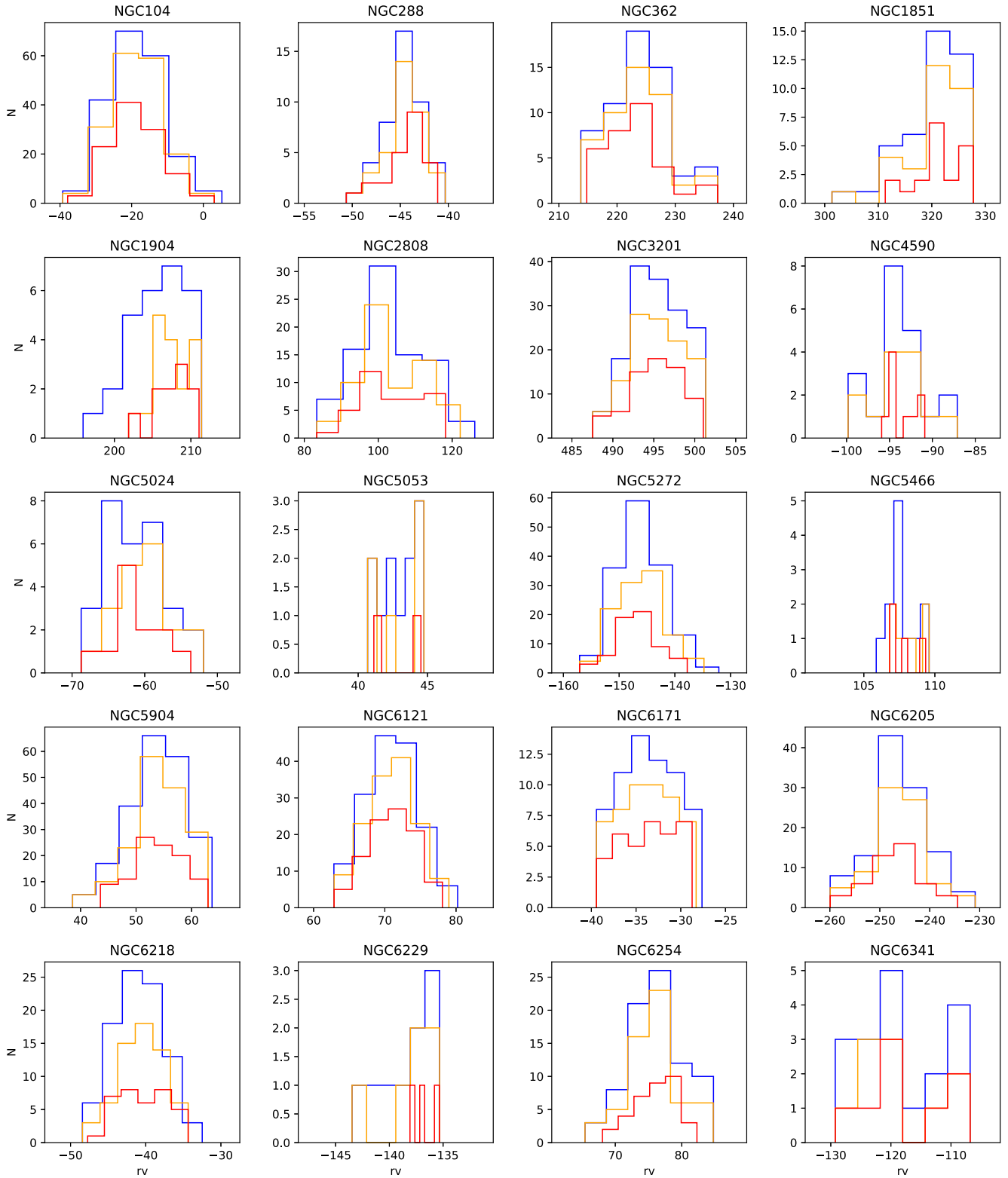
Figure A1. *–continued.*

Figure A1. –*continued.*

Figure A2. Radial velocities for the GCs in the main sample. The blue histogram represents the GC members obtained before employing the MDF sigma clip cut, for which the resulting members are highlighted as the yellow histogram. The red histogram are the resulting members after performing a second MDF sigma clip.
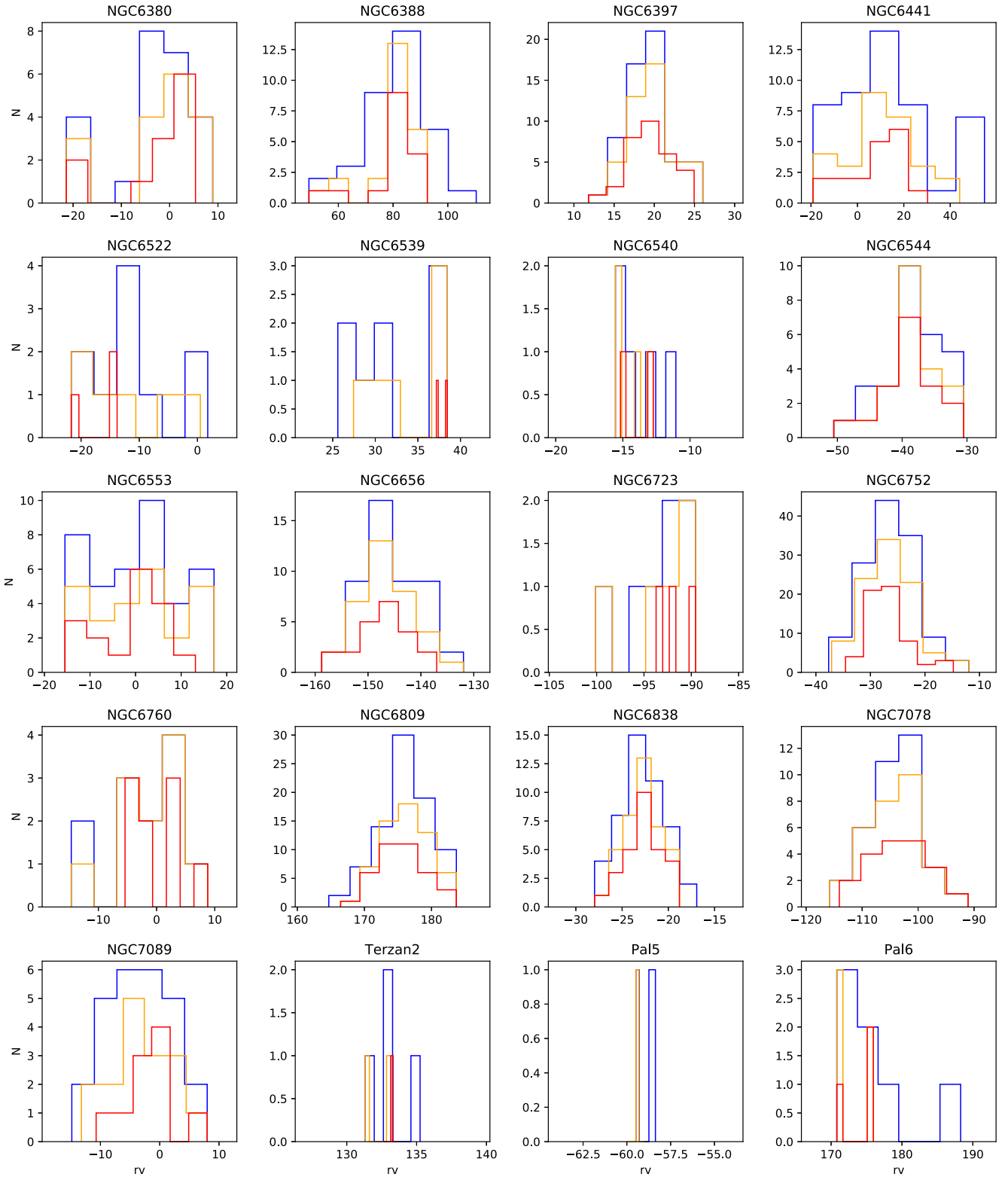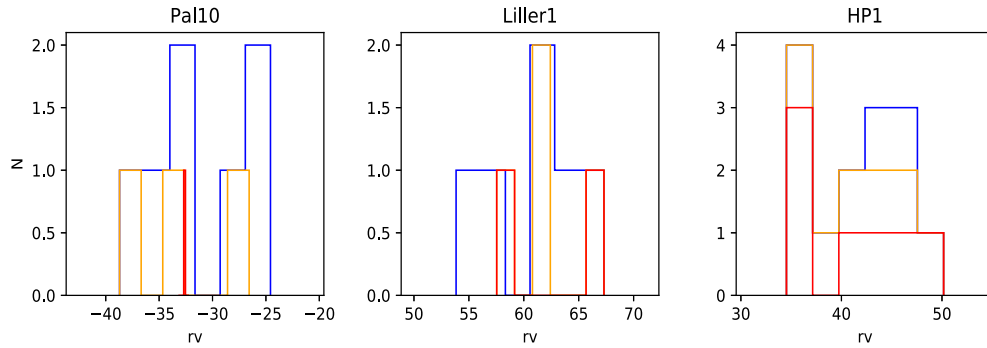
Figure A2. *–continued.*

Figure A2. *–continued.*

[1]*Astrophysics Research Institute, Liverpool John Moores University, 146 Brownlow Hill, Liverpool L3 5RF, UK*

[2]*School of Astronomy and Astrophysics, University of Birmingham, Edgbaston, Birmingham B15 2TT, UK*

[3]*Department of Physics and JINA Center for the Evolution of the Elements, University of Notre Dame, Notre Dame, IN 46556, USA*

[4]*Instituto de Astronomía y Ciencias Planetarias, Universidad de Atacama, Copayapu 485, Copiapó, Chile*

[5]*Department of Physics & Astronomy, Texas Christian University, Fort Worth, TX 76129, USA*

[6]*Instituto de Astrofísica de Canarias (IAC), E-38205 La Laguna, Tenerife, Spain*

[7]*Departamento de Astrofísica, Universidad de La Laguna (ULL), E-38206 La Laguna, Tenerife, Spain*

[8]*Departamento de Astronomía, Universidad de Concepción, Casilla 160-C, Concepción, Chile*

[9]*Departamento de Astronomía, Facultad de Ciencias, Universidad de La Serena. Av. Juan Cisternas 1200, La Serena, Chile*

[10]*New Mexico State University, Las Cruces, NM 88003, USA*

[11]*Department of Physics & Astronomy, University of Utah, Salt Lake City, UT 84112, USA*

[12]*Materials Science and Applied Mathematics, Malmö University, SE-205 06 Malmö, Sweden*

[13]*Lund Observatory, Department of Astronomy and Theoretical Physics, Lund University, Box 43, SE-22100 Lund, Sweden*

[14]*Instituto de Astronomía y Ciencias Planetarias, Universidad de Atacama, Copayapu 485, Copiapó, Chile*

[15]*Instituto de Astrofísica, Pontificia Universidad Católica de Chile, Av. Vicuna Mackenna 4860, 782-0436 Macul, Santiago, Chile*

[16]*Department of Astronomy, University of Virginia, Charlottesville, VA 22904-4325, USA*

[17]*Gothard Astrophysical Observatory, ELTE Eötvös Loránd University, 9700 Szombathely, Szent Imre H. st. 112, Hungary*

[18]*MTA-ELTE Exoplanet Research Group, 9700 Szombathely, Szent Imre H. st. 112, Hungary*

[19]*Instituto de Astronomía, Universidad Católica del Norte, Av. Angamos 0610, Antofagasta, Chile*

[20]*Department of Physics & Astronomy, The Johns Hopkins University, Baltimore, MD 21218, USA*

[21]*Departamento de Física, Facultad de Ciencias, Universidad de La Serena, Cisternas 1200, La Serena, Chile*

[22]*Centro de Astronomía (CITEVA), Universidad de Antofagasta, Avenida Angamos 601, Antofagasta 1270300, Chile*

[23]*Centre for Astrophysics Research, School of Physics, Astronomy and Mathematics, University of Hertfordshire, College Lane, Hatfield AL10 9AB, UK*

This paper has been typeset from a TEX/LATEX file prepared by the author.